Environ. Sci. Technol. **2005**, *39,* 3143−3149

Impact of the Hydrocarbon to NO_x Ratio on Secondary Organic Aerosol Formation

CHEN SONG,[†,‡] KWANGSAM NA,[†] AND DAVID R. COCKER, III*[,†,‡]

Bourns College of Engineering—Center for Environmental Research and Technology (CE-CERT), and Department of Chemical and Environmental Engineering, Bourns College of Engineering, University of California, Riverside, California 92521

A series of *m*-xylene/NO_x experiments were conducted in the new Bourns College of Engineering—Center for Environmental Research and Technology dual 90 m^3 indoor smog chamber to elucidate the role of NO_x on the secondary organic aerosol (SOA) formation potential of *m*-xylene. The results presented herein demonstrate a clear dependence of *m*-xylene SOA formation potential on NO_x, particularly at atmospherically relevant organic aerosol concentration. Experiments with lower NO_x levels generated considerably more organic aerosol mass than did experiments with higher NO_x levels when reacted *m*-xylene was held constant. For example, SOA formation from approximately 150 $\mu g\ m^{-3}$ reacted *m*-xylene produced 0.6−9.3 $\mu g\ m^{-3}$ aerosol mass for NO_x concentrations ranging from 286 to 10 ppb. The increase in SOA formation was not attributable to changes in ozone and nitrate concentration. A general discussion about possible influences of NO_x on SOA formation for this system is included.

Introduction

Aerosol formed in the atmosphere through condensation of low vapor pressure organic oxidation products is referred to as secondary organic aerosol (SOA). SOA is believed to have impacts on the radiation budget of the atmosphere related to climate change (*1*), visibility reduction (*2*, *3*), and public health (*4*, *5*). Previous studies show that SOA can significantly contribute to the atmospheric fine particle load in urban areas, especially during severe urban smog episodes. Turpin et al. (*6*) reported that 70% of the organic aerosols in Southern California were potentially SOA during the summer months, according to the Southern California Air Quality Study (SCAQS) in 1987. Na et al. (*7*) estimated that 40−67% of the organic aerosols were of secondary origin in Mira Loma, CA, from September 2001 to January 2002.

Atmospheric hydrocarbons emitted from anthropogenic sources (such as alkenes, aromatics, and carbonyls) and biogenic sources (such as terpenes and sesquiterpenes) can react with hydroxyl radical (OH), nitrate radical (NO_3), or ozone (O_3) to produce oxygenated and nitrated organic products. Products with sufficiently low vapor pressure will then partition between the gas and particle phases. Only a few percent of the chemical matrix of ambient particle phase organics have been identified due to the complexity of atmospheric organic compounds. Indirect methods have been employed to estimate SOA formation (*8*−*10*). The fractional aerosol yield (*Y*) has been widely used to represent the SOA formation potential of ambient organics (*11*, *12*). *Y* is defined as the fraction of a reactive organic gas (ROG) that is converted to aerosol and is expressed by

$$Y = M_o/\Delta\mathrm{ROG} \tag{1}$$

where M_o is the organic aerosol mass concentration ($\mu g\ m^{-3}$) and ΔROG ($\mu g\ m^{-3}$) is the reacted ROG concentration. The fractional aerosol yield was first assumed to be a constant for each ROG. Odum et al. (*13*, *14*) extended Pankow's semivolatile organic gas/particle partitioning theory (*15*, *16*) to show that the fractional aerosol yield strongly depends on the organic particulate mass. The organic particulate mass directly affects the gas/particle partitioning by acting as the medium into which oxidation products can be absorbed. Therefore, products with relatively high vapor pressure may be absorbed into the particle phase even though the products are present at concentrations below their saturation point.

In the framework developed by Odum and Pankow, a thermodynamic method combined with an empirical model has been used to analyze data for over 30 individual parent compounds obtained from the Caltech outdoor smog chamber (*13*, *14*). The results indicated that the following semiempirical two-product model was sufficiently accurate to describe the SOA yield for most parent compounds:

$$Y = M_o\left(\frac{\alpha_1 K_1}{1 + K_1 M_o} + \frac{\alpha_2 K_2}{1 + K_2 M_o}\right) \tag{2}$$

where 1 and 2 designate two lumped aerosol-forming products, one of relatively high volatility and the other of low volatility. α is the mass stoichiometric factor of compound *i* that is formed, and *K* ($m^3\ \mu g^{-1}$) is the partitioning coefficient (analogous to Henry's coefficient) in terms of the organic mass concentration, defined as

$$K_i = F_{i,\mathrm{om}}/A_i M_o \tag{3}$$

where $F_{i,\mathrm{om}}$ is the particle-phase concentration of compound *i* ($ng\ m^{-3}$) and A_i is the gas-phase concentration of compound *i* ($ng\ m^{-3}$). Since the oxidation of parent hydrocarbons can generate dozens of particle phase products, constants α_1, α_2, K_1, and K_2 have no real physical meaning and are chosen as the best fit to the smog chamber data (*13*). The chosen fit of the experimental yield data to the two-product model indicates that the four parameters satisfactorily represent the chemical stoichiometry and partitioning ability of the photooxidation product mixtures.

However, Odum's work (*13*), as well as many other smog chamber experiments, was carried out at nonatmospherically relevant conditions such as high initial reactant and NO_x concentrations. During the photooxidation process, it is difficult to identify which parameters and mechanisms involved in SOA formation are relevant to the real atmosphere. Up to now, little work has been done to investigate the role of hydrocarbons in the NO_x ratio (HC:NO_x) in SOA formation. Izumi et al. (*17*) performed two experiments with the same initial *m*-xylene concentrations but different initial NO_x concentrations, and they found similar SOA yields. Odum et al. (*13*) investigated SOA formation from *m*-xylene photooxidation with NO_x in the Caltech outdoor smog chamber and concluded that the SOA yield for *m*-xylene is weakly

* Corresponding author phone: (909) 781-5695; fax (909) 781-5790; e-mail: dcocker@cert.ucr.edu.

† CE-CERT.

‡ Department of Chemical and Environmental Engineering.

10.1021/es0493244 CCC: $30.25
Published on Web 03/11/2005

dependent on HC:NO_x. Hurley et al. (*18*) compared SOA formation from toluene and the presence of initial NO_x with that from toluene and the presence of excess NO throughout the experiment. Their study was based on several toluene/NO_x photooxidation experiments from three separate experimental facilities conducted at different temperatures and relative humidities, with variable lighting condition sources and time durations, concluding that the aerosol yield is lower with the existence of excess NO. The variable experimental conditions in earlier studies coupled with the subtle nature of the aromatic/NO_x photooxidaion system necessitate a more comprehensive experimental investigation into aerosol formation with varying NO_x levels at uniform experimental conditions. Hurley et al. (*18*) also addressed the need for future work to identify whether their results are unique to toluene oxidation or not.

It is believed that aromatic compounds may form SOA through multistep reactions with O_3, NO_3, or OH, as shown below:

$$\mathrm{HC} + \mathrm{OH} \rightarrow \alpha_1\mathrm{P}_1 + \alpha_2\mathrm{P}_2 + \alpha_3\mathrm{P}_3 + \ldots + \alpha_i\mathrm{P}_i$$

$$\mathrm{P}_i + \mathrm{OH} \rightarrow \text{condensable product}$$

$$\mathrm{P}_i + \mathrm{O}_3 \rightarrow \text{condensable product}$$

$$\mathrm{P}_i + \mathrm{NO}_3 \rightarrow \text{condensable product}$$

Because the concentrations of O_3 and NO_3 are strongly dependent on NO_x levels, changing HC:NO_x can dictate the relative reaction scheme of NO_3, OH, and O_3. This in turn will lead to different distributions of final products. The chemistry behind these aerosol formation mechanisms for aromatics is still not clear, largely due to our deficient knowledge of reaction products of aromatics under atmospheric conditions (*19*). As a result, caution should be used when the parameters obtained in smog chambers are extrapolated for predicting ambient SOA formation.

To shed light on the role of HC:NO_x acting on SOA formation, a series of experiments focusing on *m*-xylene/NO_x photooxidation were performed in the new Bourns College of Engineering—Center for Environmental Research and Technology (CE-CERT) indoor smog chamber. *m*-Xylene was selected because it is one of most abundant aromatic compounds in the urban atmosphere (*20*), it is believed to contribute to SOA formation in polluted urban areas (*10*), and it is one of the most widely studied atmospheric hydrocarbons (*21*, *22*, *30*).

Experimental Section

Facility Overview. Experiments were carried out in the new CE-CERT indoor smog chamber that is described in detail elsewhere (*23*). In this state-of-the-art system, two 90 m^3 Teflon reactors (2 mil FEP Teflon film) are suspended by a rigid steel framework in a temperature-controlled enclosure (set to 27 °C for all experiments presented herein) that is continuously flushed by purified air. Combined with an elevator, the rigid framework can be collapsed slowly during experiments to maintain a positive differential pressure between the reactors and enclosure, thus minimizing penetration of contaminants from air surrounding the reactors. Two different kinds of light sources are available: a 200 kW argon arc light and 80 115 W Sylvania 350BL blacklights. In this study, all experiments were conducted using UV irradiation with blacklight.

Pure Air System. Pure air is provided through an Aadco 737 series (Cleves, OH) air purification system followed by canisters of Purafil and heated Carulite 300 and a filter pack. Prior to each experiment, the reactor has no detectable nonmethane hydrocarbons (1 ppbC detection limit), no detectable NO_x (<10 ppt), no detectable particles (<0.2 particles cm^{-3}), and a dew point below −40 °C. The reactors are cleaned between runs by reducing the reactor volume to less than 5% of its original volume while flushing the reactors with 500 L min^{-1} of purified air.

Injection System. The initial concentration of *m*-xylene was injected into a small glass tube using a microliter syringe and was vaporized in a 50 °C pure N_2 stream. The N_2 stream then transported the *m*-xylene vapor into the chamber. Known volumes of NO were introduced into a calibrated bulb on the basis of calculated partial pressures and then flushed into the chamber by using 50 °C pure N_2 as the carrier gas. The injection and gas-phase sampling systems are located on the first floor, underneath the enclosure. This arrangement minimizes the length of gas-phase sampling and injection lines to minimize losses during transportation through the tubes.

Gas-Phase Analysis. *m*-Xylene consumption was monitored using a Hewlett-Packard 5890 (Palo Alto, CA) gas chromatograph equipped with a DB-5 column and a flame ionization detector (FID). The gas chromatography (GC) temperature program was as follows: hold at −50 °C for 2 min, increase from −50 to +40 °C at 50 °C min^{-1}, hold at 40 °C for 1 min, increase from 40 to 200 °C at 30 °C min^{-1}, and hold at 200 °C for 2.5 min. A Thermal Environmental Instruments model 42C chemiluminescence NO_x analyzer was used to measure NO, NO_y and NO_y−NO. The O_3 concentration was monitored with a Dasibi Environmental Corp. model 1003-AH O_3 analyzer. The O_3 and NO_x measurements were conducted for 10 min intervals before alternation between sides of the chamber.

Particle-Phase Analysis. The particle sampling equipment is located inside the enclosure to ensure that the instrumentation temperature is identical to the reaction temperature. The particle size distribution and number concentration were monitored using a scanning electrical mobility spectrometer consisting of a TSI model 3077 ^{85}Kr neutralizer, a TSI model 3081 long column cylindrical differential mobility analyzer (DMA), and a TSI model 3760 condensation particle counter (CPC). The DMA operates with sheath and excess flow rates of 2.5 L min^{-1} and aerosol and monodisperse flow rates of 0.25 L min^{-1}. Filtered chamber air was used for sheath air. The DMA column voltage was exponentially ramped from −40 to −7000 V to allow for measurable particle mobility size distribution in the range of 25−700 nm. The scanning electrical mobility spectrometer was operated at a 75 s scan rate and sampled alternately between two sides of the chamber.

Results and Discussion

We measured SOA formation from a series of 23 *m*-xylene/NO_x photooxidation experiments. All experiments were carried out under dry conditions (RH < 2%) in the absence of inorganic seed aerosol and were conducted until the suspended aerosol volume (corrected for wall losses) was steady. Table 1 lists the initial *m*-xylene concentration (HC_o), reacted concentration of *m*-xylene for each experiment (ΔHC), total organic aerosol mass produced (M_o), initial NO_x concentration ($NO_{x,o}$), initial mixing ratio of *m*-xylene to NO_x, final NO_x concentration ($NO_{x,f}$), experimental temperature, and overall SOA yield (Y). The total organic aerosol mass concentration was estimated from the measured total aerosol volume by assuming a density of 1 g cm^{-3} (*26*). Displayed in Figure 1 is a classic plot of SOA yield (Y) versus organic aerosol mass concentrations (M_o) for all experiments performed. The yield curve plotted in Figure 1 is obtained by minimizing the residuals between our experimental data and that calculated from the two-product semiempirical partitioning model (eq 2); experiments 247A and 247B (marked as tilted squares in Figure 1) are excluded from this calculation. The typical

TABLE 1. Experimental Conditions

run	compd	HC_o ($\mu g\ m^{-3}$)	ΔHC ($\mu g\ m^{-3}$)	M_o ($\mu g\ m^{-3}$)	$NO_{x,o}$ (ppb)	HC_o:NO_x (ppbC:ppb)	$NO_{x,f}$ (ppb)	T (K)	yield
104A	*m*-xylene	341	327.8	21.7	66.5	9.6	49.1	300	0.066
104B	*m*-xylene	341	280.9	20.4	22.7	28.2	15.5	300	0.073
107A	*m*-xylene	1196	987.5	139.7	99.0	24.0	55.0	300	0.141
107B	*m*-xylene	707	591	55.7	52.0	24.0	35.9	300	0.094
109B	*m*-xylene	677	532.1	66.3	65.0	20.0	49.0	300	0.125
129A	*m*-xylene	366	340.5	21.4	46.7	14.7	23.1	300	0.063
142A	*m*-xylene	353	302.2	21.0	46.6	14.2	34.0	300	0.070
142B	*m*-xylene	353	302.2	21.3	46.7	14.2	37.0	300	0.071
149B	*m*-xylene	719	625.7	62.6	51.0	26.5	41.3	300	0.100
154A	*m*-xylene	272	149.0	1.1	401.0	1.3	393.3	300	0.007
154B	*m*-xylene	272	263.9	10.5	61.0	8.4	45.3	300	0.040
157A	*m*-xylene	579	315.0	2.8	360.0	3.0	334.2	300	0.009
164B	*m*-xylene	289	276.7	14.3	44.8	12.1	35.4	300	0.052
217B	*m*-xylene	166	153.2	7.9	9.3	33.5	7.0	300	0.052
219B	*m*-xylene	238	166.0	9.3	9.0	49.6	7.9	300	0.056
220B	*m*-xylene	238	238.4	9.7	60.3	7.4	44.9	300	0.041
222B	*m*-xylene	234	229.9	2.5	116.0	3.8	98.0	300	0.011
223B	*m*-xylene	238	174.5	0.6	266.0	1.7	252.3	300	0.004
246A	*m*-xylene	277	204.3	16.0	14.1	36.9	10.9	300	0.078
246B	*m*-xylene	281	208.6	15.0	14.2	37.2	11.1	300	0.072
247A	*m*-xylene	1711	1660.1	131.0	586.0	5.5	368.9	300	0.079
247B	*m*-xylene	1707	1660.1	131.0	587.0	5.5	350.7	300	0.079
249B	*m*-xylene	660	642.8	20.8	240.0	5.2	187.9	300	0.032

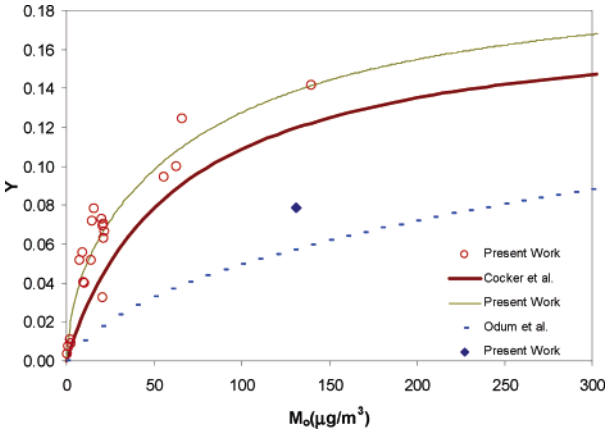

FIGURE 1. SOA yields from *m*-xylene photooxidation as a function of M_o. The solid line is fit to the experimental data of the present work (circles) using a two-product model. Values used to generate the solid line are 0.040, 0.164, 0.250, and 0.012 for α_1, α_2, K_1, and K_2, respectively. The bold line is from Cocker et al., and the dashed line is from Odum et al. The diamonds represent experiments 247A and 247B that cannot be fit to the yield curve of the present work.

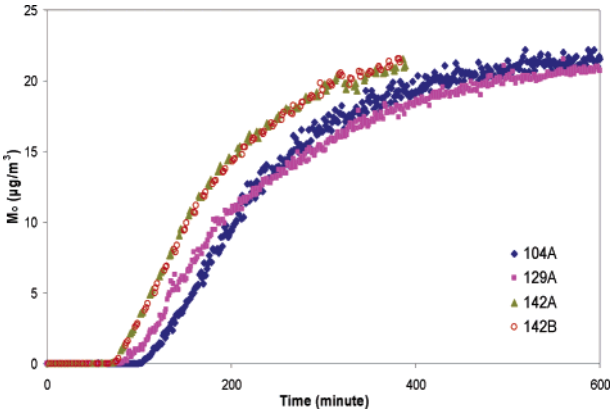

FIGURE 2. SOA mass concentrations as a function of time for four *m*-xylene photo-oxidation experiments with the same initial conditions to test run-to-run and side- to-side reproducibility. The final aerosol mass concentrations of experiments 104A, 129A, 142A, and 142B are 21.7, 21.4, 21.0, and 21.3 $\mu g\ m^{-3}$, respectively, with a standard deviation of 0.249 $\mu g\ m^{-3}$.

m-xylene concentration of urban air is about several ppbV on average (*31*). The lowest concentration in the present work is still a magnitude higher than that in the ambient, but this concentration is the lowest starting hydrocarbon concentration ever used while keeping the aerosol production significant enough for accurate measurement. Moreover, if we consider *m*-xylene as a surrogate of similar aromatic compounds such as toluene and trimethylbezenes, the low concentrations of the present work are close to those in a polluted urban atmosphere.

Comparison of the SOA Yield Curve with Previous Work. Figure 1 also displays the best-fit yield curves of *m*-xylene/NO_x photooxidations from Odum et al. (*13*) and Cocker et al. (*24*). Cocker et al.'s dataset was obtained indoors with blacklights at a temperature of approximately 293 K and a fixed 2:1 ppbC HC_o:ppb NO_x ratio. Odum et al. conducted their experiments in a 60 m^3 outdoor Teflon chamber at significantly elevated temperature (308−313 K). The lower aerosol yield curve provided by Odum et al. is consistent with the significantly higher temperatures used in their study, because K_i is inversely proportional to the pure component vapor pressure and the yield is expected to be higher at low temperature for a given M_o (*15*). However, Cocker et al.'s dataset shows an opposite behavior. While their experiments were conducted at temperatures 7 °C lower than this study, Cocker et al.'s SOA yield is still at least 14% smaller than that of the present work. It is noted that, in all of Cocker et al.'s experiments, about 300 ppb propene (not present in this work) was used to enhance photochemical reactivity. Currently, there is no literature demonstrating that propene can impact SOA formation in aromatic photooxidation systems. It should be noted that Cocker et al.'s experiments were kept at a fixed 2:1 ppbC HC_o:ppb NO_x ratio while those of the present work ranged from 1.3 to 49.6. The different behavior of Cocker et al.'s dataset will be discussed later.

Run-to-Run Reproducibility. Experiments were conducted to ensure side-to-side and run-to-run reproducibility. Figure 2 displays the wall-loss-corrected aerosol volume for four experiments (104A, 129A, 142A, and 142B). The exceptional overlap between these experiments clearly demon-

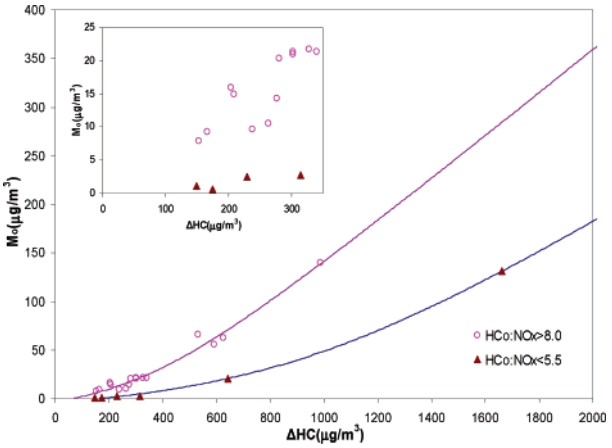

FIGURE 3. SOA mass concentrations from *m*-xylene photooxidation as a function of *m*-xylene consumption. Each data point represents a separate experiment. Also shown are calculated aerosol mass profiles by using different sets of stoichiometric and partitioning parameters. Values of α_1, α_2, K_1, and K_2 are 0.024, 0.152, 0.229, and 0.004 for low HC_o:NO_x ratio experiments (triangles) and 0.049, 0.178, 0.301, and 0.008 for high HC_o:NO_x ratio experiments (circles), respectively.

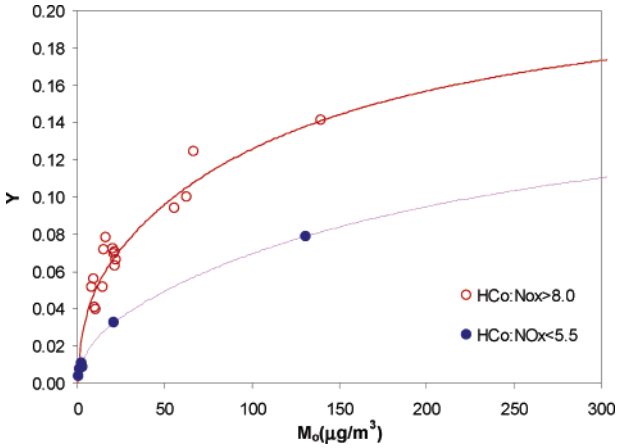

FIGURE 4. SOA yields from *m*-xylene photooxidation as a function of M_o in different NO_x regimes. Also shown are yield curves generated from a two-product model. Values of α_1, α_2, K_1, and K_2 are 0.024, 0.152, 0.229, and 0.004 for low HC_o:NO_x ratio experiments (solid circles) and 0.049, 0.178, 0.301, and 0.008 for high HC_o:NO_x ratio experiments (open circles), respectively.

strates our ability to reproducibly perform SOA experiments within the new CE-CERT chamber.

Effect of the HC:NO_x Ratio. Initial ppbC *m*-xylene to ppb NO_x ratios were varied from 1.3 to 49.6 (see Table 1). As shown in Figure 1, the two-product model can be fit through all but two of the experimental yield points obtained (R^2 = 0.90), regardless of HC:NO_x (experiments 247A and 247B were excluded from the fit and correlation as obvious outliers). Therefore, on the basis of the two-product model approach, one might assume that this indicates that the aerosol formation potential, within experimental error, is independent of HC:NO_x. Using the best-fit two-product model (shown as the solid line in Figure 1), we determined α_1, α_2, K_1, and K_2 to be 0.040, 0.164, 0.250, and 0.012, respectively. However, if we compare experiments 219B and 223B, we note that 219B produced more than 10 times more aerosol than 223B (9.7 and 0.6 μg m^{-3}, respectively) despite both experiments commencing with and consuming similar *m*-xylene concentrations (166.0 and 174.5 μg m^{-3} consumed, respectively). All reactor conditions were similar with the exception of the total NO_x levels, where experiment 219B had an initial HC:NO_x 25 times greater than that in experiment 223B. It is noted that for both experiments the aerosol growth, corrected for wall loss, plateaus prior to the end of the experiment. Despite these large differences, the yield curve still appears to fit both data points well. The dependence of SOA formation on NO_x can also be found with a closer look at Odum et al.'s work (*13*). Two experiments (08/09B and 09/13B) with similar amounts of reacted *m*-xylene and different initial NO_x levels form significantly different amounts of organic aerosol mass. Similar to that shown by the SOA yield curve of the present work, the experimental yields of Odum's 08/09B and 09/13B fall on the yield curve reported in their work.

To more easily exhibit the effect of HC:NO_x on SOA formation, we rearrange our data as a plot (Figure 3) of total organic aerosol mass produced against reacted *m*-xylene (each point represents a separate experiment). The data shown in Figure 3 remarkably fall into two distinct groups, which cannot be easily discerned from the classic yield curve as shown in Figure 1. Group 1 (triangles) consists of the results from experiments with a low ppbC *m*-xylene to NO_x ratio (defined as ppbC *m*-xylene:ppb NO_x < 5.5). Group 2 (circles) consists of experiments with a high ppbC *m*-xylene to NO_x ratio (defined as ppbC *m*-xylene:ppb NO_x > 8.0). The groupings in Figure 3 demonstrate that experiments with a higher ppbC *m*-xylene:NO_x generate significantly more organic aerosol than experiments with a higher NO_x level. A vertical slice of the figure provides the range of organic aerosol produced for a single amount of reacted *m*-xylene present and indicates that SOA formation from *m*-xylene/NO_x photooxidation can vary by more than 1 order of magnitude on the basis of the NO_x levels present. Combining eqs 1 and 2 together and solving for M_o as a function of the reacted hydrocarbon (ΔHC) yields the positive solution

$$M_o = \frac{1}{2K_1K_2}[K_1K_2(\Delta HC)(\alpha_1+\alpha_2) - (K_1+K_2) + [K_1^2K_2^2(\Delta HC)^2(\alpha_1+\alpha_2)^2 + 2K_1K_2(\Delta HC)(K_1-K_2)(\alpha_1-\alpha_2) + (K_1-K_2)^2]^{1/2}] \quad (4)$$

Now we have a new form of the semiempirical two-product model to describe the SOA formation as a function of the amount of reacted parent hydrocarbon. This new equation provides the means to easily generate two new curves from the original dataset to account for different NO_x levels. The values of α_1, α_2, K_1, and K_2 are determined to be 0.024, 0.152, 0.229, and 0.004 for group 1 (R^2 = 1.00) and 0.049, 0.178, 0.301, and 0.008 for group 2 (R^2 = 0.98), respectively. We also redisplay Figure 1 on the basis of different NO_x regimes by using the α_1, α_2, K_1, and K_2 values obtained above. As shown in Figure 4, two distinct yield curves are generated that represent low and high NO_x regimes correspondingly. It is clear that the stoichiometric and partitioning parameters decrease with elevated NO_x levels. One interpretation of this behavior is that the gas-phase chemical mechanisms are changed at different NO_x levels. In the low NO_x regime, formation of low-volatility compounds (higher K_i) is possibly more favored as well as an increase of aerosol-forming products (higher α_i). Cocker et al.'s data (*24*) fall in the high NO_x regime compared with those of the present work; the inhibition of aerosol formation in the high NO_x regime appears to overcome the enhanced aerosol formation at lower temperatures.

Unlike models that incorporate explicit gas-phase mechanisms (*28*, *29*), the two-product model is a semiempirical model based on gas−particle absorptive partitioning processes. The advantage of the two-product model is its simplicity, but the tradeoff is the lost information of specific aerosol constituents and their corresponding chemical formation mechanisms. Furthermore, as seen in Figure 1

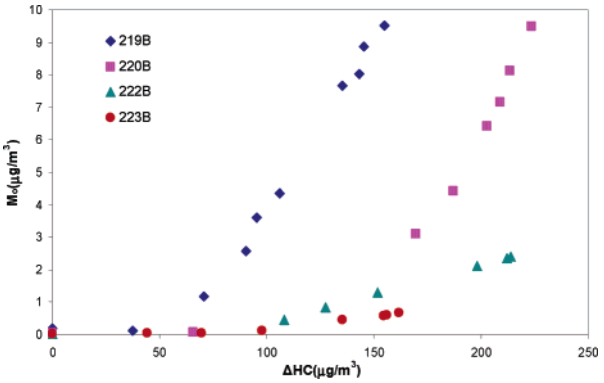

FIGURE 5. SOA mass concentrations from the photooxidation of *m*-xylene as a function of *m*-xylene consumption for four experiments with different NO_x levels.

and Odum et al.'s *m*-xylene yield curve (*13*), it may be difficult to use yield curves (Y vs M_o) to identify the effect of NO_x on aerosol formation. This difficulty is overcome for experiments performed at unrealistically high reactant and NO_x concentrations. However, the generated α_i and K_i parameters may not be directly applicable to atmospheric conditions. For example, Atkinson (*19*) suggests that the reaction of OH−aromatic adducts with NO_2 can be an important or even dominant chemical pathway in laboratory product studies at high NO_x concentrations, whereas they are of minor importance in the troposphere.

Mechanism for the NO_x Effect. Under atmospheric conditions, degradation of *m*-xylene is predominantly initiated by reaction with OH adding to the aromatic ring (*30*), which produces a variety of primary compounds that may undergo further chemical oxidation to generate condensable species. Previous researchers (*22*, *25*, *26*) found that a number of ring-opening and ring-retaining products are formed during photooxidation of aromatic precursors. Such ring-opening and ring-retaining products may contain one or more double bonds that may further react with O_3, NO_3, or OH. The final distribution of condensable species may then depend on the chemical oxidation route (based on the relative attack of O_3, NO_3, or OH), leading to varied SOA mass concentrations. A previous study of toluene/NO_x photooxidation by Hurley et al. (*18*) suggested that the existence of high NO_x levels suppressed ozone formation and that aerosol formation was predominately through reactions with the OH. They suggested that their low NO_x level experiments promoted O_3 and NO_3 formation, compounds that subsequently reacted with toluene oxidation products, increasing aerosol formation in addition to the aerosol produced from reaction with the OH. We compared four of our experiments to explore Hurley et al.'s hypothesis that O_3 and NO_3 contribute to aerosol formation. Our four experiments had the same initial *m*-xylene concentration (50 ppb) but varied NO_x concentrations (9.0−266 ppb). They are illustrated in Figures 5 and 6. Figure 5 shows the aerosol mass concentration as a function of *m*-xylene consumption, and Figure 6 displays the measured gas trace evolutions. A couple of striking features are shown in Figure 5. An obvious delay of SOA formation from initial consumption of *m*-xylene is observed, indicating that SOA is produced through secondary reactions of the primary gaseous products (*27*). Moreover, the different initial consumptions of *m*-xylene required before SOA formation in these experiments imply that SOA may not be generated in each experiment from the same secondary reaction routes. This is further supported by the varying aerosol formation at different NO_x levels seen for each of the four experiments. Among these experiments, 220B has the highest O_3 concentration while 219B has the highest SOA yield. Experiment 222B also has considerably higher O_3 concentration than 219B, but its SOA yield is about 5 times less. During the photooxidation process, NO is converted to NO_2, resulting

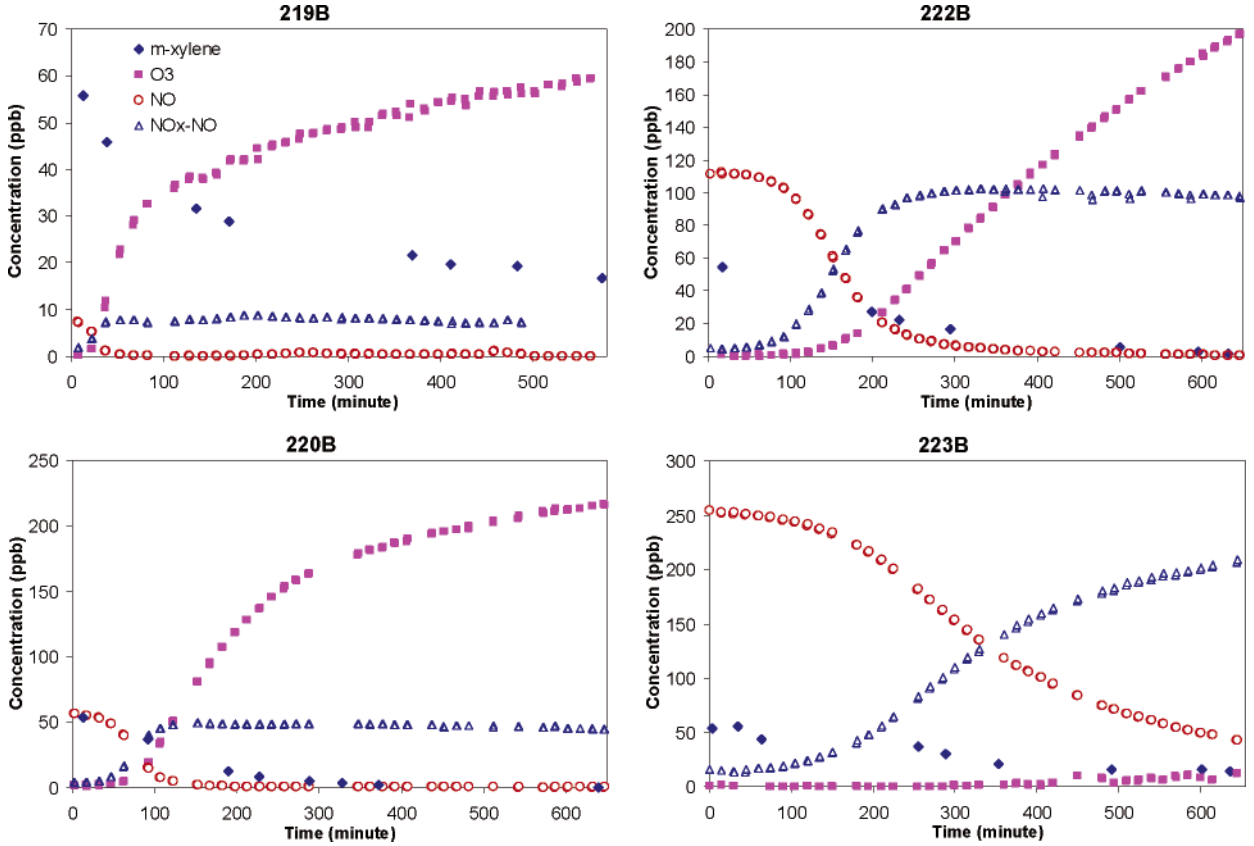

FIGURE 6. Observed concentrations of *m*-xylene, NO, NO_x−NO, and O_3 as a function of time for experiments 219B, 220B, 222B, and 223B.

in O_3 formation. NO_2 and O_3 then react to form NO_3, which means NO_3 concentration is dictated by the O_3 and NO_2 concentrations. Since 220B and 222B have higher O_3 and NO_2 concentrations than 219B, the NO_3 levels should be expected to be higher for 220B and 222B than for 219B. If OH, O_3, and NO_3 are the only reason for SOA formation, 220B and 223B should have higher SOA yields than 219B because of their higher OH, O_3, and NO_3 concentrations. Therefore, the discussion above leads to the interpretation that the SOA yield is only slightly dependent on or unaffected by O_3 and NO_3 existing in the smog chamber.

As mentioned previously, oxidation products from *m*-xylene and OH reaction are substantially formed from ring-retaining or ring-opening pathways. The ring-retaining pathway generates phenol-like products such as dimethylphenols that have recently been shown to have very high SOA yields (up to 60%) with the presence of NO_x (*31*). Primary products from the ring-opening pathway include 4-oxo-2-pentenal, glyoxal, and methylglyoxal (*22*). Volkamer et al. (*32*) report that the phenol yield from benzene and OH reaction is about twice as high as that from previous studies under atmospherically relevant NO_x concentrations. Further investigation (*33*) indicated that the phenol yield decreased at elevated NO_x concentrations (> 100 ppb) and ring-opening products are favored. Although this result was obtained from benzene, it should also be applied to other aromatics such as *m*-xylene. So the explanation for the significant differences in aerosol formation between low and high NO_x experiments is possibly due to the different yields of dimethylphenols. Additional data, particularly aerosol speciation under different NO_x regimes, are necessary to support this hypothesis. Another potential interpretation, based on the growing attention on heterogeneous reactions (*34*, *35*), is that differing NO_x levels may impact the heterogeneous reactions occurring in the aerosol by altering the precursors (aldehydes, ketones, and alcohols) that are necessary for heterogeneous reactions.

Although we have investigated the dependence of SOA formation potential on the NO_x level from only a single aromatic photooxidation, this behavior is expected to exist in other aromatic hydrocarbon−NO_x systems as well. Further analysis on the role of NO_x in SOA formation at low organic aerosol loadings is imperative to assess the global and local impacts of different hydrocarbons.

Acknowledgments

We gratefully acknowledge funding support from National Science Foundation Grant ATM-0234111. We thank Kurt Bumiller, Irina Malkina, and Jean Wang for their help with the experiment setup and measurement, and William P. L. Carter for helpful discussions.

Literature Cited

(1) Pilinis, C.; Pandis, S.; Seinfeld, J. H. Sensitivity of direct climate forcing by atmospheric aerosols to aerosol size and composition. *J. Geophys. Res.* **1995**, *100*, 18739−18754.

(2) Eldering, A.; Cass, G. R. Source-oriented model for air pollutant effects on visibility. *J. Geophy. Res.* **1996**, *101*, 19343−19369.

(3) Larson, S. M.; Cass, G. R. Characteristics of summer midday low-visibility events in the Los Angeles area. *Enivron. Sci. Technol.* **1989**, *23* (3), 281−289.

(4) Schwartz, J.; Dockery, D. W.; Neas, L. M.; et al. Is daily mortality associated specifically with fine particles? *J. Air Waste Manage. Assoc.* **1996**, *46*, 927−39.

(5) EPA. *Air Quality Criteria for Particulate Matter*; EPA/600/P-95/001cF; Environmental Protection Agency: Washington, DC, 1996.

(6) Turpin, B. J.; Huntzicker, J. J. Secondary formation of organic aerosol in the Los-angles basin−a descriptive analysis of organic and elemental carbon concentrations. *Atmos. Environ.* **1991**, *25A* (2), 207−215.

(7) Kwangsam, Na; Aniket, A.; Swant, C. S.; Cocker, D. R., III. Primary and secondary carbonaceous species in the atmosphere of Western Riverside County, California. *Atmos. Environ.* **2004**, *38*, 1345−1355.

(8) Turpin, B. J.; Huntzicker, J. J. Identification of secondary organic aerosol episodes and quantitation of primary and secondary organic aerosol concentrations during SCAQS. *Atmos. Environ.* **1995**, *29*, 3527−44.

(9) Turpin, B. J.; Huntzicker, J. J.; Larson, S. M.; Cass, G. R. Los Angeles summer midday particulate carbon: primary and secondary aerosol. *Enivron. Sci. Technol.* **1991**, *25*, 1788−93.

(10) Pandis, S. N.; Harley, R. A.; Cass, G. R.; Seifeld, J. H. Secondary organic aerosol formation and transport. *Atmos. Environ.* **1992**, *26A* (13), 2269−82.

(11) Grosjean, D.; Seinfeld, J. H. Parameterization of the formation potentialo of secondary organic aerosols. *Atmos. Environ.* **1989**, *23*, 1733−1747.

(12) Pandis, S. N.; Wexler, A. S.; Seinfeld, J. H. Secondary organic aerosol formation and transport .2. Predicting the ambient secondary organic aerosol-size distribution. *Atmos. Environ.* **1993**, *27A*, 2403−2416.

(13) Odum, J. R.; Hoffmann, T.; Bowman, F.; Collins, D.; Flagan, R. C.; Seinfeld, J. H. Gas/particle partitioning and secondary organic aerosol yields. *Environ. Sci. Technol.* **1996**, *30*, 2580−85.

(14) Odum, J. R.; JungKamp, T. P. W.; Griffin, R. J.; Forstner, H. J. L.; Flagan, R. C.; Seinfeld, J. H. Aromatics, reformulated gasoline, and atmospheric organic aerosol formation. *Environ. Sci. Technol.* **1997**, *31*, 1890−97.

(15) Pankow, J. F. An absorption-model of gas-particle partitioning of organic-compounds in the atmosphere. *Atmos. Environ.* **1994**, *28* (2), 185−188.

(16) Pankow, J. F. An absorption-model of the gas aerosol partitioning involved in the formation of secondary organic aerosol. *Atmos. Environ.* **1994**, *28* (2), 189−193.

(17) Izumi, K.; Fukuyama, T. Photochemical aerosol formation from aromatic-hydrocarbons in the presence of NO_x. *Atmos. Environ.* **1990**, *24A* (6), 1433−1441.

(18) Hurley, M. D.; Sokolov, O.; Wallington, T. J.; Takekawa, H.; Karasawa, M.; Klotz, B.; Barnes, I.; Becker, K. H. Organic aerosol formation during the atmospheric degradation of toluene. *Environ. Sci. Technol.* **2001**, *35*, 1358−1366.

(19) Atkinson, R. *J.* Atmospheric chemistry of VOCs and NO_x. *Atmos. Environ.* **2000**, *34*, 2063−2101.

(20) Jefferies, H. E. Photochemical Air Pollution. In *Composition, Chemistry, and Climate of the Atmosphere*; Singh, H. B., Ed.; Van Nostrand Reinhold: New York, 1995.

(21) Atkinson, R.; Aschmann, S. M.; Arey, J. Formation of ring-retaining products from the OH radical-initated reactions of *o*-, *m*-, and *p*-xylene. *Int. J. Chem. Kinet.* **1991**, *23*, 77−97.

(22) Smith, D. F.; Kleindienst, T. E.; McIver, C. D. Primary product distributions from the reaction of OH with *m*-, *p*-xylene, 1,2,4- and 1,3,5-trimethylbenzene. *J. Atmos. Chem.* **1999**, *34*, 339−364.

(23) Carter, W. P. L.; Cocker, D. R., III; Fitz, D. R.; Malkina, I. L.; Bumiller, K.; Sauer, C. G.; Pisano, J. T.; Bufalino, C.; Song, C. A new environmental chamber for evaluation of gas- phase chemical mechanisms and secondary aerosol formation. Submitted to *Atmos. Environ.*, in press.

(24) Cocker, D. R., III; Mader, B. T.; Kalberer, M.; Flagan, R. C.; Seinfeld, J. H. The effect of water on gas−particle partitioning of secondary organic aerosol: II. *m*-xylene and 1,3,5-trimethylbenzene photooxidation systems. *Atmos. Environ.* **2001**, *35*, 6073−6085.

(25) Jang, M.; Kamens, R. M. Characterization of secondary aerosol from the photooxidation of toluene in the presence of NO_x and 1-propene. *Environ. Sci. Technol.* **2001**, *35*, 3626−3639.

(26) Forstner, H. J. L.; Flagan, R. C.; Seinfeld, J. H. Secondary organic aerosol from the photooxidation of aromatic hydrocarbons: molecular composition. *Environ. Sci. Technol.* **1997**, *31*, 1345−1358.

(27) Bowman, F. M.; Odum, J. R.; Seinfeld, J. H. Mathematical model for gas-particle partitioning of secondary organic aerosols. *Atmos. Environ.* **1997**, *31* (23), 3921−3931.

(28) Carter, W. P. L. *Documentation of the SAPRC-99 Chemical Mechanism for VOC Reactivity Assessment*; Final Report to California Air Resources Board; Contract Nos. 92-329 and 95-308; 2000.

(29) University of Leeds Master Chemical Mechanism version 3.1, http://mcm.leeds.ac.uk/MCM/home.htt.

(30) Calvert, J. G.; Atkinson, R.; Becker, K. H.; Kammens, R. M.; Seinfeld, J. H.; Wallington, T. J.; Yarwood, G. *The Mechanisms of Atmospheric Oxidation of Aromatic Hydrocarbons*; Oxford University Press: Oxford, 2002.

(31) Thüner, L. P.; Rea, G.; Wenger, J. In *2nd EUPHORE Report 2000*; Barnes, I., Sidebottom, H., Eds.; Institute of Physical Chemistry, Bergische Universität Wuppertal: Wuppertal, Germany, 2001; pp 39−44.

(32) Volkamer, R.; Klotz, B.; Barnes, I.; Imamura, T.; Wirtz, K.; Washida, N.; Becker, K. H.; Platt, U. OH-initiated oxidation of benzene. Part I. Phenol formation under atmospheric conditions. *Phys. Chem. Chem. Phys.* **2002**, *4*, 1598−1610.

(33) Klotz, B.; Volkamer, R.; Hurley, M. D.; Andersen, M. P. S.; Nielsen, O. J.; Barnes, I.; Imamura, T.; Wirtz, K.; Becker, K.; Platt, U.; Wallington, T. J.; Washida, N. OH-initiated oxidation of benzene. Part II. Influence of elevated NO_x concentrations. *Phys. Chem. Chem. Phys.* **2002**, *4*, 4399−4411.

(34) Jang, M.; Czoschke, N. M.; Lee, S.; Kamens, R. M. Heterogeneous atmospheric aerosol production by acid-catalyzed particle-phase reactions. *Science* **2002**, *298*, 814−817.

(35) Kalberer, M.; Paulsen, D.; Sax, M.; Steinbacher, M.; Dommen, J.; Prevot, S. H.; Fisseha, R.; Weingartner, R.; Frankevich, V.; Zenobi, R.; Baltensperger, U. Identification of polymers as major components of atmospheric organic aerosols. *Science* **2004**, *303*, 1659−1662.

Received for review May 3, 2004. Revised manuscript received January 8, 2005. Accepted February 3, 2005.

ES0493244